VIP Photocatalysis Very Important Paper

DOI: 10.1002/anie.201410172

# One-pot Synthesis of CdS Nanocrystals Hybridized with Single-Layer Transition-Metal Dichalcogenide Nanosheets for Efficient Photocatalytic Hydrogen Evolution**

*Junze Chen, Xue-Jun Wu, Lisha Yin, Bing Li, Xun Hong, Zhanxi Fan, Bo Chen, Can Xue, and Hua Zhang**

***Abstract:*** *Exploration of low-cost and earth-abundant photocatalysts for highly efficient solar photocatalytic water splitting is of great importance. Although transition-metal dichalcogenides (TMDs) showed outstanding performance as co-catalysts for the hydrogen evolution reaction (HER), designing TMD-hybridized photocatalysts with abundant active sites for the HER still remains challenge. Here, a facile one-pot wet-chemical method is developed to prepare $MS_2$–CdS ($M$ = W or Mo) nanohybrids. Surprisedly, in the obtained nanohybrids, single-layer $MS_2$ nanosheets with lateral size of 4–10 nm selectively grow on the Cd-rich (0001) surface of wurtzite CdS nanocrystals. These $MS_2$–CdS nanohybrids possess a large number of edge sites in the $MS_2$ layers, which are active sites for the HER. The photocatalytic performances of $WS_2$–CdS and $MoS_2$–CdS nanohybrids towards the HER under visible light irradiation (> 420 nm) are about 16 and 12 times that of pure CdS, respectively. Importantly, the $MS_2$–CdS nanohybrids showed enhanced stability after a long-time test (16 h), and 70 % of catalytic activity still remained.*

The conversion of solar energy into chemical fuels by photocatalytic water splitting using semiconductors as catalysts is considered as one of the most promising ways to solve the energy crisis and global environmental problems.[1] Since the first report on using $TiO_2$ as catalyst for photoinduced water splitting in 1972,[2] a large number of semiconductor materials have been developed for the photocatalytic hydrogen evolution reaction (HER).[3–8] Among them, CdS has attracted great attention because of its optimal band gap (about 2.4 eV) for effective absorption of sunlight, a relatively simple production method, and suitable conduction band for the HER.[9–11] However, CdS showed an extremely low activity for the photocatalytic hydrogen production and poor stability because of the charge carrier recombination and its photocorrosion.[12]

Loading of co-catalysts on semiconductor photocatalysts is an effective way to inhibit the charge carrier recombination, which greatly improves the catalyst activities.[12,13] Several co-catalysts have been developed to integrate with CdS to form composites, such as CdS–Pt,[14] CdS–Au,[15] CdS–NiO,[16] and CdS–$Cu_2S$,[17] which have shown promising results. As another kind of co-catalysts, layered transition-metal dichalcogenide (TMD) nanosheets, such as $MS_2$ ($M$ = W or Mo),[18] exhibited excellent performance towards electrocatalytic hydrogen evolution.[19,20] It is well-known that the edge sites of TMD nanosheets are the active sites for the HER.[21–23] Therefore, optimally engineering TMD to preferentially expose active edge sites significantly enhanced their activity for the HER.[24–26] Till now, several reports have demonstrated the integration of CdS nanomaterials with TMD nanosheets to form the p/n junction, which achieved enhanced performance towards the photocatalytic hydrogen production under visible light irradiation.[27–30] However, their used TMD nanosheets with large lateral sizes or multi-layered structures greatly limited their activity towards the HER owing to the low exposure of active edge sites. Therefore, synthesis of photocatalysts containing single-layer TMD nanosheets with a large number of active sites is still required.

Herein, we report a facile one-pot wet-chemical method to fabricate $MS_2$–CdS ($M$ = W or Mo) nanohybrids, in which the single-layer TMD selectively grew on the Cd-rich (0001) surface of wurtzite CdS nanocrystals. The lateral size of single-layer TMD is 4–10 nm, leading to a large percentage of active surface sites of TMD. Importantly, the obtained nanohybrids showed enhanced photocatalytic performances compared to the pure CdS nanoparticles. Moreover, the $MS_2$–CdS catalyst also showed good stability. About 70 % of the catalytic activity were still maintained after it was irradiated with visible light for long time (16 h).

The $MS_2$–CdS nanohybrids were synthesized through a hot-injection method (see the Experimental Section for details). The transmission electron microscopy (TEM) image reveals that the $WS_2$–CdS nanohybrids are quite uniform with

[*] J. Chen, Dr. X.-J. Wu, L. Yin, Dr. X. Hong, Z. Fan, B. Chen, Prof. C. Xue, Prof. H. Zhang
School of Materials Science and Engineering
Nanyang Technological University
50 Nanyang Avenue, Singapore 639798 (Singapore)
E-mail: hzhang@ntu.edu.sg
hzhang166@yahoo.com
Homepage: http://www.ntu.edu.sg/home/hzhang/
Dr. B. Li
Institute of Materials Research and Engineering
A*STAR (Agency for Science, Technology and Research)

[**] This work was supported by MOE under AcRF Tier 2 (ARC 26/13, grant number MOE2013-T2-1-034), AcRF Tier 1 (grant numbers RG 61/12, RGT18/13, and RG5/13), and Start-Up Grant (grant number M4080865.070.706022) in Singapore, and National Research Foundation in Siangapore. This Research is also conducted by NTU-HUJ-BGU Nanomaterials for Energy and Water Management Programme under the Campus for Research Excellence and Technological Enterprise (CREATE), that is supported by the National Research Foundation, Prime Minister's Office, Singapore.

Supporting information for this article is available on the WWW under http://dx.doi.org/10.1002/anie.201410172.

  

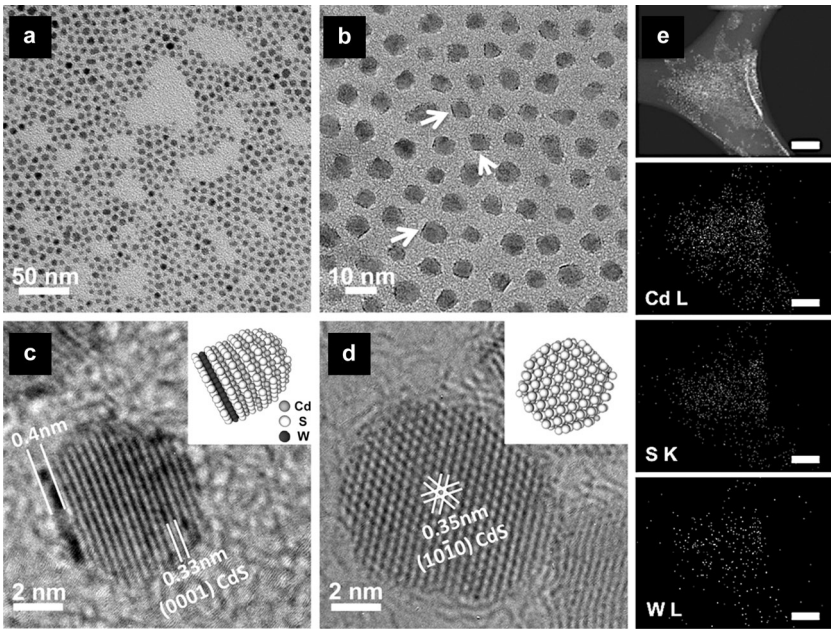


***Figure 1.*** TEM images and STEM-EDS mapping of $WS_2$–CdS nanohybrids. a,b) TEM images of $WS_2$–CdS. The white arrows in (b) indicate the single-layer $WS_2$ nanosheets, which grew on the Cd-rich (0001) surface of CdS nanocrystals. c,d) HR-TEM images of $WS_2$–CdS nanohybrids viewed perpendicularly and parallelly to the *c* axis of CdS nanocrystals, respectively, as shown in the respective insets in (c) and (d). e) Dark-field STEM image and the corresponding EDS mapping of $WS_2$–CdS nanohybrids (scale bars = 100 nm).

particle size of 4–10 nm (Figure 1 a). Very interestingly, some individual nanoparticles show different contrast in high-magnification TEM image (Figure 1 b), that is, single-layer nanosheets (indicated by white arrows) selectively grown on CdS nanocrystals. These single-layer nanosheets were confirmed to be $WS_2$ (see the description below). Powder X-ray diffraction (XRD) measurement was used to determine the structure of as-synthesized nanohybrids. All diffraction peaks can be indexed to hexagonal CdS with wurtzite structure (JCPDS No.04-004-5012) with cell parameters of $a = 0.412$ nm and $c = 0.669$ nm (see Figure S1 in the Supporting Information). However, $WS_2$ does not show any obvious peaks in the XRD pattern, which can be attributed to its single-layer structure. In Figure 1 c,d, the observed inter-plane distances between lattice fringes are measured to be 0.33 and 0.35 nm, which are perfectly in agreement with those between the adjacent {0002} and $\{10\bar{1}0\}$ planes of hexagonal CdS, respectively. Importantly, the single-layer $WS_2$ with thickness of about 0.4 nm can be clearly observed in the high-resolution TEM (HR-TEM) image (Figure 1 c), viewed perpendicularly to the c axis of the CdS nanocrystal (inset of Figure 1 c), which is in good accord with the distance between two S layers of a single-layer $WS_2$ nanosheet.[31]

Because of the unique morphology of the $WS_2$–CdS nanohybrid, its detailed structure needs to be determined. It is well-known that CdS with wurtzite structure contains alternating Cd and S atom layers along the [0001] direction. Therefore, the exposed {0001} planes are terminated either by a Cd-rich (0001) surface or S-rich $(000\bar{1})$ surface. The anionic sulfur donors, such as $MoS_4^{2-}$ or $Et_2NCS_2$, preferentially adsorb on the Cd-rich surface.[32] Therefore, it is reasonable to conclude that the single-layer $WS_2$ selectively grows on the Cd-rich (0001) surface of CdS, which has strong interaction with the S layer of $WS_2$. The inset of Figure 1 c schematically shows a representative sketch image of this unique structure. Unfortunately, the $WS_2$ layer cannot be clearly observed if the electron beam irritated parallelly along the *c* axes of CdS because of its ultrathin characteristic (Figure 1 d). Furthermore, STEM-EDS was performed to confirm the composition of the obtained nanohybrids (Figure 1 e). The dark-field image shows the $WS_2$–CdS nanohybrids are uniformly distributed on the copper grid. The corresponding EDS elemental mapping also reveals the homogeneous distribution of Cd, S, and W elements. The molar ratio of W to Cd was determined to be 11:100 based on the EDS analysis (Figure S2).

To investigate the shape evolution of such unique nanohybrids, a series of time-dependent experiments have been carried out through characterizing the aliquots from the reaction flask at different time intervals. The thermal decomposition of $(NH_4)_2WS_4$ involves two distinct steps.[33,34] The first step results in the formation of $WS_3$ and releases $H_2S$ molecules [Reaction (1)]. In the second step, the as-formed

$$(NH_4)_2WS_4 = WS_3 + 2\,NH_3 + H_2S \quad (1)$$

$WS_3$ further decomposes to $WS_2$ and S [Reaction (2)].

$$WS_3 = WS_2 + S \quad (2)$$

Compared with the second decomposition step, the first step is much easier to proceed and occurs at relatively low temperature (about 180 °C).[34] Considering that there is no additional sulfur source used in the synthesis, $(NH_4)_2WS_4$ not only acts as the precursor which decomposes to form $WS_2$, but also provides a sulfur source for the nucleation and growth of CdS nanocrystals.

Figure 2 a–c gives the typical TEM images of products obtained at different reaction time. At short reaction time, such as 5 minutes, only small $WS_2$ clusters (about 1 nm) decorated on the surface of CdS nanoparticles were observed (Figure 2 a). As the reaction continuously proceeded, $WS_3$ continuously decomposed to produce $WS_2$. The small $WS_2$ clusters continuously grew and fused together at a reaction time of 30 minutes (Figure 2 b). At a reaction time of 1 hour, $WS_2$ nanomaterials further evolved into smooth, continuous, single-layer $WS_2$ nanosheets, which selectively grew on the Cd-rich (0001) surface of CdS nanocrystals (Figure 2 c). In this reaction, the Ostwald ripening and/or the oriented attachment processes played a very important role in the whole evolution process.[35]

  

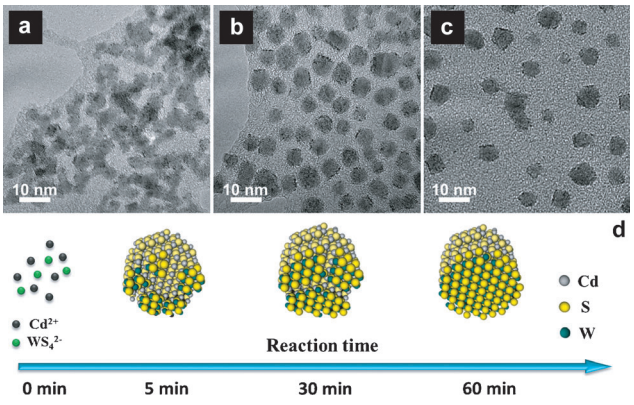


***Figure 2.*** TEM images of $WS_2$–CdS nanohybrids obtained at different reaction time. The reaction time is a) 5, b) 30, c) 60 minutes. d) Schematic illustration of the shape evolution of $WS_2$–CdS nanohybrids.

Impressively, our method can also be used to synthesize $MoS_2$–CdS nanohybrids by replacing $(NH_4)_2WS_4$ with $(NH_4)_2MoS_4$. In the obtained $MoS_2$–CdS nanohybrids, single-layer $MoS_2$ nanosheets also selectively grew on the Cd-rich (0001) surface of CdS nanocrystals. The low-resolution TEM images showed the $MoS_2$–CdS nanohybrids with a size of 6–11 nm (Figure 3a). Single-layer $MoS_2$ nanosheets can be clearly observed in the enlarged TEM image (Figure 3b, indicated by white arrows). HR-TEM images showed four representative nanohybrids, viewed perpendicularly to the *c* axes of CdS nanocrystals, and single-layer $MoS_2$ nanosheets with thickness of about 0.4 nm were clearly observed (Figure 3c). The observed interplane distance between the lattice fringes is about 0.33 nm, corresponding to the {0001} planes of wurtzite CdS. The XRD pattern also confirmed the presence of hexagonal wurtzite CdS (Figure S3). The molar ratio of Mo to Cd was determined to be 7:100 based on the EDS analysis (Figure S4), which is similar to that of $WS_2$–CdS nanohybrids (11:100). The binding energies of elements in $MoS_2$–CdS nanohybrids were further characterized by the X-ray photoelectron spectroscopy (XPS; Figure S5). The high-resolution spectra of Mo 3d, S 2p, and Cd 3d were measured to determine the oxidation states of these elements. The peaks of Mo 3d appear at binding energy of 228.9 eV ($Mo3d_{5/2}$) and 232.1 eV ($Mo3d_{3/2}$), indicating that $Mo^{4+}$ is the dominant oxidation states. In addition, the two peaks of S 2p are located at 161.9 eV and 163.1 eV, respectively, which can be assigned to the presence of sulfide. The binding energies of Mo and S are in good agreement with the previous report,[36] confirming the presence of $MoS_2$. The high-resolution Cd 3d spectra contain two peaks centered at 405.7 eV ($Cd3d_{5/2}$) and 412.5 eV ($Cd3d_{3/2}$), indicating the typical divalent source of Cd from CdS.[37]

The lateral size of single-layer $WS_2$ and $MoS_2$ nanosheets grown on CdS nanocrystals is typically less than 10 nm, which could significantly increase the exposure area of active edge sites. Furthermore, the size of $MS_2$–CdS nanohybrids is also quite small (from 4–11 nm), which shortens the diffusion pathway of charge carriers and thus decreases the probability of charge carrier recombination. Meanwhile, the p/n junction formed between the single-layer TMD nanosheet and CdS nanoparticle in the $MS_2$–CdS nanohybrids accelerates the separation of electron-hole pairs. Therefore, a better HER performance is expected for these unique nanohybrids.

Photocatalytic hydrogen evolution activities of $WS_2$–CdS and $MoS_2$–CdS nanohybrids were evaluated under visible light irradiation ($\lambda > 420$ nm) using lactic acid as the hole scavenger. Figure 4a,b summarizes the hydrogen evolution rates using pure CdS, $WS_2$–CdS, and $MoS_2$–CdS nanohybrids as catalysts. Obviously, the amount of hydrogen steadily increases with time (Figure 4a). The pure CdS shows the lowest photocatalytic activity, while both nanohybrids show

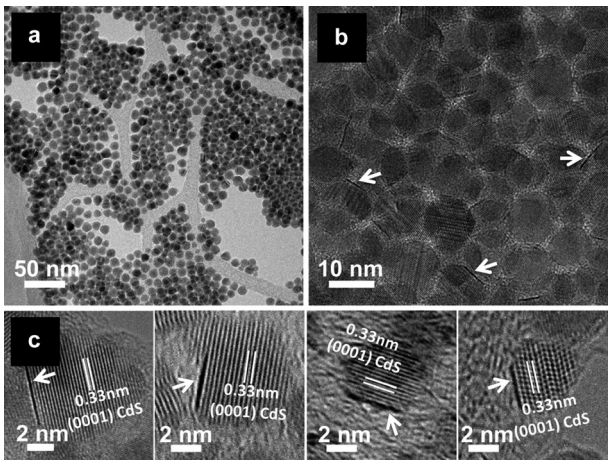


***Figure 3.*** TEM images of $MoS_2$–CdS nanohybrids. a,b) Low-resolution TEM images of $MoS_2$–CdS nanohybrids. c) Representative HR-TEM images of $MoS_2$–CdS viewed perpendicularly to the *c* axis of CdS nanocrystals. The white arrows in (b) and (c) indicate the single-layer $MoS_2$ nanosheets which grew on the Cd-rich (0001) surface of CdS nanocrystals.

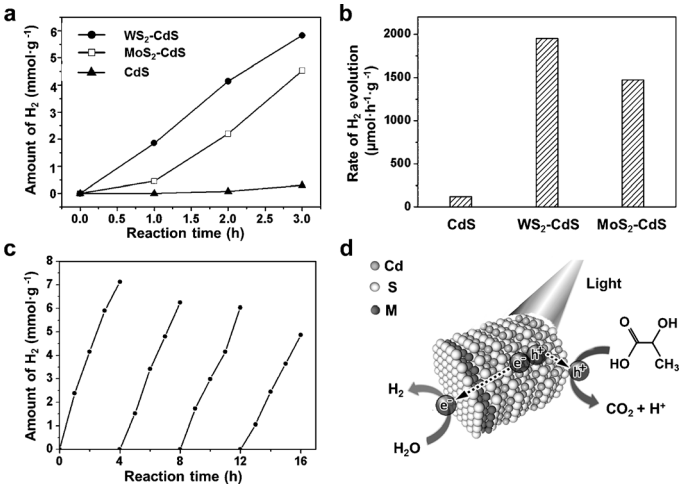


***Figure 4.*** Photocatalytic activity of $MS_2$–CdS nanohybrids for Hydrogen evolution reaction. a) Time-dependent photocatalytic $H_2$ evolution for $WS_2$–CdS, $MoS_2$–CdS, and pure CdS. b) Comparison of the $H_2$-evolution rate under visible light irritation for $WS_2$–CdS, $MoS_2$–CdS, and pure CdS. c) Cycling test of photocatalytic $H_2$ evolution for $WS_2$–CdS. d) Schematic illustration of the photocatalytic process of $MS_2$–CdS nanohybrids in the lactic acid solution.

enhanced activities. The hydrogen evolution rates of $WS_2$–CdS and $MoS_2$–CdS nanohybrids are 1984 and 1472 μmol $h^{-1}$ $g^{-1}$ (Figure 4b), nearly 16 and 12 times that of pure CdS (119 μmol $h^{-1}$ $g^{-1}$), respectively.

To investigate the stability of $WS_2$–CdS nanohybrids, four consecutive photocatalytic reactions were performed and each reaction was carried out under visible light irritation for 4 h (Figure 4c). The amount of generated hydrogen increased steadily with the irradiation time in each cycle. Although the photocatalytic activity decreased after 16 h of irradiation, 70% of catalytic activity still remained. The gradual deterioration of catalytic activity for the nanohybrids mainly arises from the photocorrosion of CdS during the photocatalytic reaction, which is a major problem for metal sulfide photocatalysts.[30] Figure 4d schematically illustrates the photocatalytic process of the nanohybrids. Upon photoexcitation, the electron–hole pairs can be generated in the CdS nanoparticle. The electrons diffuse to the single-layer TMD nanosheet because of the inherent p/n junction, and directly react with $H^+$ in water to produce $H_2$ at its active sites. Meanwhile, the holes are mainly consumed by the lactic acid to generate $CO_2$.

In summary, we have developed a facile one-pot wet-chemical method to prepare $MS_2$–CdS ($M$ = W, Mo) nanohybrids. In the obtained nanohybrids, single-layer $MS_2$ nanosheets selectively grew on the Cd-rich (0001) surface of wurtzite CdS nanocrystals. The $MS_2$–CdS nanohybrids showed excellent photocatalytic activity towards the HER with quite good stability, arising from the large number of active sites of single-layer $MS_2$ nanosheets and the inherent p/n heterojunction formed between $MS_2$ and CdS. This method could be used for preparation of other TMD–CdS nanohybrids or even TMD–semiconductor nanohybrids for future clean energy applications.

## Experimental Section

Chemicals: Cadmium oxide (CdO, 99.99%, Puratrem), ammonium tetrathiomolybdate ($(NH_4)_2MoS_4$, 99.97%, Sigma-Aldrich), ammonium tetrathiotungstate ($(NH_4)_2WS_4$, 99.9%, Sigma–Aldrich), oleic acid (OA, 90%, Sigma–Aldrich), oleylamine (OM, technical grade, 70%, Sigma–Aldrich), 1-octadecene (ODE, technical grade, 90%, Sigma–Aldrich), Trioctylphosphine (TOP, 97%, Sigma–Aldrich), 3-mercaptopropionic acid (MPA, 99%, Sigma–Aldrich), toluene (99.8%, Sigma–Aldrich), acetone (technical grade), and methanol (AR) were used as received without further purification. The Milli-Q water (Milli-Q System, Millipore, Billerica, MA) was used in some experiments.

Synthesis of $WS_2$–CdS nanohybrids: Into a mixture composed of 9 mL of ODE, 3 mL of OM, and 3 mL of OA in a three-necked flask (100 mL), 0.3 mmol of CdO were added at room temperature. The slurry was heated to 120 °C to remove water and oxygen with vigorous magnetic stirring under vacuum for 30 minutes in a temperature-controlled mantle. After the mixture was purged with nitrogen and heated up to 300 °C, 2 mL of 0.05 M $(NH_4)_2WS_4$ oleylamine stock solution was quickly injected into the mixture. The temperature was dropped to 280 °C and then went back to 300 °C again which was maintained for 2 h. When the mixture was cooled to room temperature, the nanohybrids were precipitated by addition of acetone and then collected by centrifugation. They were washed by the mixture of toluene and acetone for three times.

The 0.05 M $(NH_4)_2WS_4$ oleylamine stock solution was prepared by mixing 0.5 mmol of $(NH_4)_2WS_4$ (174 mg) and 10 mL of OM in a 25 mL bottle, which was heated to 80 °C and then kept for 5 h.

Synthesis of $MoS_2$–CdS nanohybrids: The procedures for the synthesis of $MoS_2$–CdS nanohybrids are similar to those for the synthesis of $WS_2$–CdS nanohybrids. The 0.05 M $(NH_4)_2MoS_4$ oleylamine stock solution was prepared by mixing 0.5 mmol of $(NH_4)_2MoS_4$ and 10 mL of OM in a 25 mL bottle, which was heated to 80 °C and then kept for 5 h. Into a mixture of 9 mL of ODE, 3 mL of OM and 3 mL of OA in a three-necked flask (100 mL), 0.3 mmol of CdO were added at room temperature. The slurry was heated to 120 °C to remove water and oxygen with vigorous magnetic stirring under vacuum for 30 minutes in a temperature-controlled mantle. After the mixture was purged with nitrogen and heat up to 280 °C, 2 mL of 0.05 M $(NH_4)_2MoS_4$ oleylamine stock solution were quickly injected into the mixture. After it was kept at 280 °C for 2 h under stirring, it was cooled down to room temperature. The $MoS_2$–CdS nanohybrids were precipitated by addition of acetone and then collected by centrifugation. They were washed by the mixture of toluene and acetone for three times.

Characterization: Powder XRD patterns of the dried products were recorded on Shimadzu XRD-6000 with a slit of (1/2)° at a scanning rate of 2° $min^{-1}$, using Cu Ka radiation ($\lambda = 1.5406$ Å). Samples for TEM characterizations were prepared by dropping the nanohybrid dispersion in toluene on amorphous carbon-coated copper grids. TEM characterization was performed with a JEOL 2010F (Japan) or JEOL 2100F (Japan) operated at 200 kV. Samples for EDS analyses were prepared by dropping the nanohybrid dispersion in toluene on copper grids (for $WS_2$–CdS) or Si/SiO2 substrate (for $MoS_2$–CdS). The EDS measurements were performed with JEOL JSM-7600F. XPS measurements were carried out on a VG ESCALAB 220I-XL system. A thick nanohybrid film was prepared on a Si substrate by drop-casting of the nanohybrid solution in toluene.

Preparation of the water-soluble nanohybrids: The synthesized $MS_2$–CdS nanohybrid in toluene was transferred to water solution by MPA-assisted phase transfer method.[38] After 5 mL of toluene containing 20 mg $MS_2$–CdS were added into a 10 mL glass bottle, 5 mL of 10 vol% MPA water solution were added into it under vigorous stirring. After 2 h, the nanohybrids were transferred to water phase. The MPA-coated $MS_2$–CdS nanohybrids were collected by centrifugation and washed three times with Milli-Q water to remove excess MPA.

Photocatalytic hydrogen evolution: The photocatalytic activity was evaluated using water soluble MPA-coated $MS_2$–CdS nanohybrids as photocatalysts, 10 mg of MPA-coated $WS_2$–CdS photocatalysts were suspended in 10 mL aqueous solution containing 10% of lactic acid as the sacrificial agent. The suspension was sealed in a glass vessel and purged with nitrogen for 30 minutes to remove oxygen. After degassing, the vessel was exposed under a 300 W xenon lamp (MAX-302, Asahi Spectra Company, Led.) coupled with a UV cutoff filter (> 420 nm) to evaluate the photocatalytic activity under the visible-light irradiation. The $H_2$ product was analyzed periodically by gas chromatograph (GC, Agilent 7890A) with a thermal conductivity detector (TCD).

Received: October 16, 2014
Published online: December 3, 2014

**Keywords:** heterojunctions · hydrogen evolution · nanocrystals · nanohybrids · photocatalysis

[1] N. S. Lewis, D. G. Nocera, *Proc. Natl. Acad. Sci. USA* **2006**, *103*, 15729–15735.
[2] A. Fujishima, *Nature* **1972**, *238*, 37–38.
[3] A. Kudo, Y. Miseki, *Chem. Soc. Rev.* **2009**, *38*, 253–278.

  

[4] F. E. Osterloh, *Chem. Mater.* **2007**, *19*, 35 – 54.
[5] X. Chen, S. Shen, L. Guo, S. S. Mao, *Chem. Rev.* **2010**, *110*, 6503 – 6570.
[6] Y. Sun, Z. Sun, S. Gao, H. Cheng, Q. Liu, J. Piao, T. Yao, C. Wu, S. Hu, S. Wei, Y. Xie, *Nat. Commun.* **2012**, *3*, 1057.
[7] Y. Sun, H. Cheng, S. Gao, Z. Sun, Q. Liu, Q. Liu, F. Lei, T. Yao, J. He, S. Wei, Y. Xie, *Angew. Chem. Int. Ed.* **2012**, *51*, 8727 – 8731; *Angew. Chem.* **2012**, *124*, 8857 – 8861.
[8] F. Lei, Y. Sun, K. Liu, S. Gao, L. Liang, B. Pan, Y. Xie, *J. Am. Chem. Soc.* **2014**, *136*, 6826 – 6829.
[9] Y. Li, L. Tang, S. Peng, Z. Li, G. Lu, *Crystengcomm* **2012**, *14*, 6974 – 6982.
[10] T. Peng, K. Li, P. Zeng, Q. Zhang, X. Zhang, *J. Phys. Chem. C* **2012**, *116*, 22720 – 22726.
[11] C. Nasr, S. Hotchandani, W. Y. Kim, R. H. Schmehl, P. V. Kamat, *J. Phys. Chem. B* **1997**, *101*, 7480 – 7487.
[12] R. Marschall, *Adv. Funct. Mater.* **2014**, *24*, 2421 – 2440.
[13] Z. Zhu, J. Guo, W. Liu, Z. Li, B. Han, W. Zhang, Z. Tang, *Angew. Chem. Int. Ed.* **2013**, *52*, 13571 – 13575; *Angew. Chem.* **2013**, *125*, 13816 – 13820.
[14] H. Park, W. Choi, M. R. Hoffmann, *J. Mater. Chem.* **2008**, *18*, 2379 – 2385.
[15] X. Ma, K. Zhao, H. Tang, Y. Chen, C. Lu, W. Liu, Y. Gao, H. Zhao, Z. Tang, *Small* **2014**, DOI: 10.1002/smll.201401494.
[16] Z. Khan, M. Khannam, N. Vinothkumar, M. De, M. Qureshi, *J. Mater. Chem.* **2012**, *22*, 12090 – 12095.
[17] M. Sam, M. Bayati, M. Mojtahedi, K. Janghorban, *Appl. Surf. Sci.* **2010**, *257*, 1449 – 1453.
[18] Z. Zeng, Z. Yin, X. Huang, H. Li, Q. He, G. Lu, F. Boey, H. Zhang, *Angew. Chem. Int. Ed.* **2011**, *50*, 11093 – 11097; *Angew. Chem.* **2011**, *123*, 11289 – 11293.
[19] X. Huang, Z. Zeng, S. Bao, M. Wang, X. Qi, Z. Fan, H. Zhang, *Nat. Commun.* **2013**, *4*, 1444.
[20] D. Voiry, H. Yamaguchi, J. Li, R. Silva, D. C. Alves, T. Fujita, M. Chen, T. Asefa, V. B. Shenoy, G. Eda, *Nat. Mater.* **2013**, *12*, 850 – 855.
[21] T. F. Jaramillo, K. P. Jørgensen, J. Bonde, J. H. Nielsen, S. Horch, I. Chorkendorff, *Science* **2007**, *317*, 100 – 102.
[22] H. I. Karunadasa, E. Montalvo, Y. Sun, M. Majda, J. R. Long, C. J. Chang, *Science* **2012**, *335*, 698 – 702.
[23] B. Hinnemann, P. G. Moses, J. Bonde, K. P. Jørgensen, J. H. Nielsen, S. Horch, I. Chorkendorff, J. K. Nørskov, *J. Am. Chem. Soc.* **2005**, *127*, 5308 – 5309.
[24] J. Kibsgaard, Z. Chen, B. N. Reinecke, T. F. Jaramillo, *Nat. Mater.* **2012**, *11*, 963 – 969.
[25] J. Xie, H. Zhang, S. Li, R. Wang, X. Sun, M. Zhou, J. Zhou, X. W. D. Lou, Y. Xie, *Adv. Mater.* **2013**, *25*, 5807 – 5813.
[26] D. Kong, H. Wang, J. J. Cha, M. Pasta, K. J. Koski, J. Yao, Y. Cui, *Nano Lett.* **2013**, *13*, 1341 – 1347.
[27] X. Zong, H. Yan, G. Wu, G. Ma, F. Wen, L. Wang, C. Li, *J. Am. Chem. Soc.* **2008**, *130*, 7176 – 7177.
[28] J. Zhang, Z. Zhu, X. Feng, *ACS Nano* **2014**, *8*, 7078 – 7087.
[29] C. Zhu, X. Mu, P. A. van Aken, Y. Yu, J. Maier, *Chem. Eur. J.* **2014**, *20*, 10632 – 10635.
[30] X. Zong, H. Yan, G. Wu, G. Ma, F. Wen, L. Wang, C. Li, *J. Phys. Chem. C* **2011**, *115*, 12202 – 12208.
[31] C. Zhu, X. Mu, P. A. van Aken, Y. Yu, J. Maier, *Angew. Chem. Int. Ed.* **2014**, *53*, 2152 – 2156; *Angew. Chem.* **2014**, *126*, 2184 – 2188.
[32] J. J. Hickman, M. S. Wrighton, *J. Am. Chem. Soc.* **1991**, *113*, 4440 – 4448.
[33] A. Müller, T. Prasad, R. Menge, *Z. Anorg. Allg. Chem.* **1972**, *391*, 107 – 112.
[34] T. Prasad, E. Diemann, A. Müller, *J. Inorg. Nucl. Chem.* **1973**, *35*, 1895 – 1904.
[35] C. Schliehe, B. H. Juarez, M. Pelletier, S. Jander, D. Greshnykh, M. Nagel, A. Meyer, S. Foerster, A. Kornowski, C. Klinke, *Science* **2010**, *329*, 550 – 553.
[36] H. Wang, P. Skeldon, G. Thompson, *Surf. Coat. Technol.* **1997**, *91*, 200 – 207.
[37] X. Chen, X. Huang, L. Kong, Z. Guo, X. Fu, M. Li, J. Liu, *J. Mater. Chem.* **2010**, *20*, 352 – 359.
[38] R. Xie, U. Kolb, J. Li, T. Basché, A. Mews, *J. Am. Chem. Soc.* **2005**, *127*, 7480 – 7488.

  